Photon statistics of intense entangled photon pulses

2013 J. Phys. B: At. Mol. Opt. Phys. 46 175502

(http://iopscience.iop.org/0953-4075/46/17/175502)

J. Phys. B: At. Mol. Opt. Phys. **46** (2013) 175502 (11pp) doi:10.1088/0953-4075/46/17/175502

Photon statistics of intense entangled photon pulses

Frank Schlawin and Shaul Mukamel

Department of Chemistry, University of California, Irvine, CA 92697-2025, USA

E-mail: Frank.Schlawin@physik.uni-freiburg.de and smukamel@uci.edu

Received 11 April 2013, in final form 10 June 2013
Published 19 August 2013
Online at stacks.iop.org/JPhysB/46/175502

Abstract
Time- and frequency-gated two-photon counting is given by a four-time correlation function of the electric field. This reduces to two times with purely time gating. We calculate this function for entangled photon pulses generated by parametric down-conversion. At low intensity, the pulses consist of well-separated photon pairs, and crossover to squeezed light as the intensity is increased. This is illustrated by the two-photon absorption signal of a three-level model, which scales linearly for a weak pump intensity where both photons come from the same pair, and gradually becomes nonlinear as the intensity is increased. We find that the strong frequency correlations of entangled photon pairs persist even for higher photon numbers. This could help facilitate the application of these pulses to nonlinear spectroscopy, where these correlations can be used to manipulate congested signals.

(Some figures may appear in colour only in the online journal)

1. Introduction

Entangled photons have become an invaluable resource in quantum optics with possible applications to cryptography [1], lithography [2], metrology [3] and quantum computing [4, 5]. Applications to spectroscopy received considerable attention in experiments [6–9] as well as in theoretical works [10–16]. These prospects necessitate the adaption of quantum information concepts to spectroscopic applications. Four wave mixing signals with quantum fields depend on integrals containing a product of a four-point dipole correlation function of matter and a four-point correlation function of the field [12]. In spectroscopic applications, the latter provide an observation window for the former. This window is more complex than what is possible with classical light. Understanding the field correlation functions and their manipulation should help in the design of novel spectroscopic techniques involving quantum light.

Photon statistics are most commonly measured by purely time gating, and characterized by the G_2-function, a four-point field correlation function evaluated at two times [17, 18]. Four-wave mixing spectroscopy signals with entangled light depend on the same correlation function, but at four different times [12]. This can be measured by time- and frequency-gated photon statistics.

Here, we investigate the normally ordered four-time correlation function $\langle E^\dagger(\tau_1)E^\dagger(\tau_2)E(\tau_3)E(\tau_4)\rangle$ of type-II down-converted photons using the formalism derived in [19, 20], which generalizes the work of Mandel and co-workers in the 1980s [21, 22]. Quantum noise is not considered [23–25]. Our approach allows us to describe the intensity dependence of the four-point correlation function in the continuous-mode limit. We assess the time- and frequency-resolution offered by this function, by application to the Hong–Ou–Mandel (HOM) interferometer [26, 27]. The two-photon absorption (TPA) signal in a three-level system represents a nonlinear measurement that can exploit the properties of the nonclassical correlation function. We further describe the transition between the linear and nonlinear scaling regimes of TPA with pump intensity, and calculate the crossover intensity. The linear (rather than quadratic) scaling of the four-point correlation function of the field with the pump intensity [7, 28, 29] enables nonlinear spectroscopy at very low input fluxes, thus minimizing damage to photosensitive samples.

2. Parametric down-conversion

We consider type-II parametric down-conversion (PDC) in a birefringent crystal. A pump photon of frequency ω_p is split into two photons with frequencies ω_1 and ω_2 and orthogonal

polarizations, such that $\omega_p = \omega_1 + \omega_2$ [30, 31]. Due to their different polarization, the photon wavepackets travel at different group velocities inside the crystal, and acquire a relative time delay during their propagation, which is bound by the entanglement time T. If T is very short, the bandwidth of the individual beams can exceed that of the pump, in which case the two photons are time-frequency entangled. In this paper, we will restrict our attention to degenerate down-conversion, where the central frequencies of the two down-converted beams coincide.

2.1. The model

PDC involves three broadband fields: a pump field E_p, and the two generated fields E_1 and E_2. Each of these fields contains a continuum of frequencies, and is described by the operator

$$\hat{E}_i(t) = \int \frac{\mathrm{d}\omega_i}{2\pi} \mathcal{A}(\omega_i)\hat{a}_i(\omega_i)\,\mathrm{e}^{-\mathrm{i}\omega_i t} \quad i \in \{p, 1, 2\}, \tag{1}$$

where $\hat{a}(\omega)$ is the photon annihilation operator, and $\mathcal{A}(\omega) = \sqrt{\hbar\omega/(4\pi\epsilon_0 cA)}$, where c is the speed of light, and A denotes the transverse quantization area [32]. We adopt the slowly varying envelope approximation, where we assume that the bandwidth of the fields is much smaller than their central frequencies. This allows us to approximate the factor $\mathcal{A}(\omega)$ as constant, $\mathcal{A}(\omega) \approx \mathcal{A}(\omega_0)$. The down-conversion process within the birefringent crystal is described by the unitary evolution operator [19]

$$U_{\mathrm{PDC}}(t) = \mathcal{T}\exp\left[-\frac{\mathrm{i}}{\hbar}\int^t \mathrm{d}\tau H_{\mathrm{int},I}(\tau)\right], \tag{2}$$

with

$$H_{\mathrm{int}}(t) = \epsilon_0 \int_{-L/2}^{L/2} \mathrm{d}z\, \chi^{(2)}(z)E_p(z,t)E_1^\dagger(z,t)E_2^\dagger(z,t). \tag{3}$$

Here, we assume collinear geometry of the three fields, such that the interaction is restricted to the crystal length L in the propagation direction of the fields. The second-order susceptibility $\chi^{(2)}$ [1] is assumed to be constant in space, and independent of frequency. We further assume that the pump field is very strong, i.e. it does not get depleted by the interaction in the crystal. We can therefore replace its field operator $E_p(t)$ by the field envelope $A_0A_p(\omega)\,\mathrm{e}^{-\mathrm{i}\omega_p t}$, where A_p is normalized as $\int \mathrm{d}\omega A_p(\omega) = 1$, and A_0 denotes the pump strength. The remaining Hamiltonian acts only on the fields E_1 and E_2. If we neglect time-ordering and take the limit $t \to \infty$, we can carry out the time integration, and obtain an effective Hamiltonian for the down conversion process [19]

$$\begin{aligned} |\psi_f\rangle &= U_{\mathrm{PDC}}|\psi_i\rangle, \\ U_{\mathrm{PDC}} &\simeq \exp\left[-\frac{\mathrm{i}}{\hbar}H_{\mathrm{eff}}\right], \end{aligned} \tag{4}$$

$$H_{\mathrm{eff}} = \int \mathrm{d}\omega_a \int \mathrm{d}\omega_b\; \Phi(\omega_a,\omega_b)a^\dagger(\omega_a)b^\dagger(\omega_b) + \mathrm{h.c.} \tag{5}$$

with

$$\Phi(\omega_a,\omega_b) = \alpha A_p(\omega+\omega_b)\mathrm{sinc}\left(\frac{\Delta k(\omega_a,\omega_b)L}{2}\right). \tag{6}$$

[1] Strictly speaking, the coefficient is similar to $\chi^{(2)}$, but is not the same [33].

Here, $|\psi_i\rangle$ and $|\psi_f\rangle$ represent the state of the field before and after passing through the PDC crystal, respectively. We shall assume that the fields are initially in the vacuum state, $|\psi_i\rangle = |0\rangle_1 \otimes |0\rangle_2$. A_p is the (normalized) pump envelope, and the phase mismatch $\Delta k(\omega_a,\omega_b)$ is given by [34]

$$\Delta k(\omega_a,\omega_b)L = \frac{(\omega_a-\omega_p/2)T_1}{2} + \frac{(\omega_b-\omega_p/2)T_2}{2}, \tag{7}$$

where $T_1 = (1/v_p = 1/v_1)L$, and $T_2 = (1/v_p = 1/v_2)L$. v_i denotes the group velocity of the ith beam at its central frequency. The entanglement time is then given by $T = T_2 - T_1$.

The conversion efficiency is given by

$$\alpha = \frac{A_0\epsilon_0\chi^{(2)}L}{2}\mathcal{A}(\omega_1)\mathcal{A}(\omega_2)\left(\frac{1}{2\pi}\right)^3, \tag{8}$$

where ω_i are the central frequencies of fields 1 and 2.

To calculate the propagator U_{PDC} in a closed form, we perform the singular value decomposition (SVD) of the two-photon envelope [35],

$$-\frac{\mathrm{i}}{\hbar}\Phi(\omega_a,\omega_b) \equiv \sum_k r_k\psi_k^*(\omega_a)\phi_k^*(\omega_b). \tag{9}$$

Here, $r_k \geqslant 0$ are the singular values, and the functions $\{\psi_k\}$ and $\{\phi_k\}$ form orthonormal bases. We further define the time domain envelopes

$$u_k(t) = \int \frac{\mathrm{d}\omega}{2\pi}\,\psi_k^*(\omega)\,\mathrm{e}^{-\mathrm{i}\omega t}, \tag{10}$$

$$v_k(t) = \int \frac{\mathrm{d}\omega}{2\pi}\,\phi_k^*(\omega)\,\mathrm{e}^{-\mathrm{i}\omega t}. \tag{11}$$

In appendix A, we use the SVD to calculate U_{PDC} (equation (4)), which is then used to calculate the four-point field correlation function in the frequency domain.

3. Time- and frequency-gated two-photon counting

We will consider with the Hong, Ou and Mandel setup as depicted in figure 1, where the entangled beams are mixed in a balanced beamsplitter, and beam 2 is delayed by δt. This is described by the transformation of the down-converted fields

$$E_a(t) = E_1(t) + E_2(t+\delta t), \tag{12}$$

and

$$E_b(t) = E_1(t) - E_2(t+\delta t). \tag{13}$$

The time- and frequency-gated two-photon counting signal of beams a and b is given by a convolution of the 'bare signal' S_B with the spectrograms W_D of the two detectors [36, 37],

$$\begin{aligned} S(\bar{t}_i,\bar{\omega}_i,\bar{t}_s,\bar{\omega}_s;\delta t) = \int \mathrm{d}t_i \int \mathrm{d}t_s \int \frac{\mathrm{d}\omega_i}{2\pi}\int \frac{\mathrm{d}\omega_s}{2\pi} \\ W_D^i(t_i,\omega_i;\bar{t}_i,\bar{\omega}_i)W_D^s(t_s,\omega_s;\bar{t}_s,\bar{\omega}_s) \\ S_B(t_i,\omega_i;t_s,\omega_s;\delta t), \end{aligned} \tag{14}$$

where the bare signal is given by

$$\begin{aligned} S_B(t_i,\omega_i;t_s,\omega_s;\delta t) = \int \mathrm{d}\tau_i\,\mathrm{e}^{-\mathrm{i}\omega_i\tau_i}\int \mathrm{d}\tau_s\,\mathrm{e}^{-\mathrm{i}\omega_s\tau_s} \\ \times\left\langle E_a^\dagger(t_i+\tau_i)E_b^\dagger(t_s+\tau_s)E_b(t_s)E_a(t_i)\right\rangle \end{aligned} \tag{15}$$

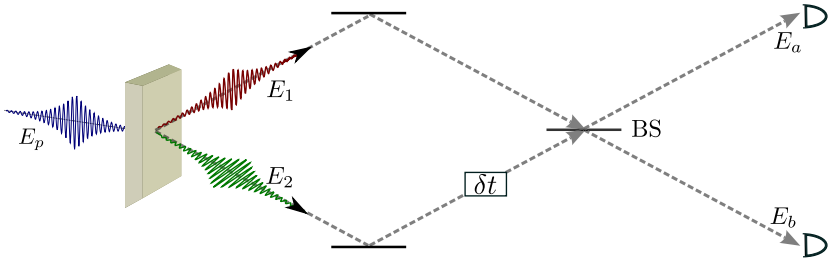

Figure 1. The HOM interferometer, equation (18). The two beams are mixed at a balanced beam splitter, and correlation events of the two detectors are recorded.

$$= -\int \frac{\mathrm{d}\omega_a}{2\pi}\int \frac{\mathrm{d}\omega_a}{2\pi}\,\mathrm{e}^{\mathrm{i}((\omega_i-\omega_a)t_i+(\omega_s-\omega_b)t_s)} \times\langle E_a^\dagger(\omega_i)E_b^\dagger(\omega_s)E_b(\omega_b)E_a(\omega_a)\rangle. \tag{16}$$

Here, the dependence on the time delay δt is implicit in the definition of the fields E_a and E_b (equations (12) and (13)). We shall use the following model for the detector spectrogram:

$$W_D(t,\omega;\bar{t},\bar{\omega}) = \frac{W}{\sigma_D}\,\mathrm{e}^{-\frac{(t-\bar{t})^2}{T^2}}\,\mathrm{e}^{-\frac{(\omega-\bar{\omega})^2}{\sigma_D^2}}. \tag{17}$$

Here, $\sigma_D^2 = 1/\bar{T}^2 + \Omega^2$, with $\bar{T}$ the time resolution and Ω the frequency resolution. Using equations (12) and (13), the correlation function appearing in the bare signal reads

$$\begin{aligned}
&\langle E_a^\dagger(t_i+\tau_i)E_b^\dagger(t_s+\tau_s)E_b(t_s)E_a(t_i)\rangle\\
&= \langle E_1^\dagger(t_i+\tau_i)E_1^\dagger(t_s+\tau_s)E_1(t_s)E_1(t_i)\rangle\\
&\quad+\langle E_2^\dagger(t_i+\tau_i+\delta t)E_2^\dagger(t_s+\tau_s+\delta t)E_2(t_s+\delta t)E_2(t_i+\delta t)\rangle\\
&\quad+\langle E_1^\dagger(t_i+\tau_i)E_2^\dagger(t_s+\tau_s+\delta t)E_2(t_s+\delta t)E_1(t_i)\rangle\\
&\quad-\langle E_1^\dagger(t_i+\tau_i)E_2^\dagger(t_s+\tau_s+\delta t)E_1(t_s)E_2(t_i+\delta t)\rangle\\
&\quad-\langle E_2^\dagger(t_i+\tau_i+\delta t)E_1^\dagger(t_s+\tau_s)E_2(t_s+\delta t)E_1(t_i)\rangle\\
&\quad+\langle E_2^\dagger(t_i+\tau_i+\delta t)E_1^\dagger(t_s+\tau_s)E_1(t_s)E_2(t_i+\delta t)\rangle.
\end{aligned} \tag{18}$$

These correlation functions are evaluated in appendix A.

3.1. Pure time gating

Conventional photon statistics with high temporal and no spectral resolution are described by the limit $\bar{T}\to 0$, which yields the detector spectrogram

$$\mathrm{e}^{-\frac{(t-\bar{t})^2}{\bar{T}^2}} \longrightarrow \delta(t-\bar{t}), \tag{19}$$

and

$$\mathrm{e}^{-\frac{(\omega-\bar{\omega})^2}{\sigma_D^2}} \longrightarrow 1. \tag{20}$$

This enables us to evaluate equation (14) as

$$\begin{aligned}
&S(\bar{t}_i,\bar{t}_s;\delta t)\\
&= \left|\sum_k \sinh(r_k)\cosh(r_k)\left(u_k(\bar{t}_i)v_k(\bar{t}_s+\delta t)-u_k(\bar{t}_s)v_k(\bar{t}_i+\delta t)\right)\right|^2\\
&\quad+\left|\sum_k \sinh^2(r_k)\left(u_k(\bar{t}_i)u_k^*(\bar{t}_s)-v_k(\bar{t}_i+\delta t)v_k^*(\bar{t}_s+\delta t)\right)\right|^2\\
&\quad+\left(\sum_k \sinh^2(r_k)\left(u_k(\bar{t}_s)u_k^*(\bar{t}_s)+v_k(\bar{t}_s+\delta t)v_k^*(\bar{t}_s+\delta t)\right)\right)\\
&\quad\times\left(\sum_k \sinh^2(r_k)\left(u_k(\bar{t}_i)u_k^*(\bar{t}_i)+v_k(\bar{t}_i+\delta t)v_k^*(\bar{t}_i+\delta t)\right)\right).
\end{aligned} \tag{21}$$

Since we have eliminated the $\bar{\omega}_s$ and $\bar{\omega}_i$ indices, the signal now only depends on two times $\bar{t}_i$ and $\bar{t}_s$. Only the first line in equation (21), which is $\propto(\sinh(r_k)\cosh(r_k))^2$ and is linear in the intensity, contributes for a weak pump. It constitutes the coherent interaction of entangled photon pairs; ψ_f in this limit is known as a twin-photon state. The signal can be understood as the interference between pathways, where both photons are reflected or transmitted, respectively [38] (see also figure 2(a)). When the two beams create indistinguishable photons, this term is responsible for the celebrated HOM-dip.

To leading order, the second term in equation (21) scales quadratically in the pump intensity, and therefore shows up only for stronger pump fields. It is created by the beam splitter, but in contrast to the first term, it corresponds to an interference between terms, where both photons stem from either beam 1 or beam 2.

Finally, the third term in equation (21) can be factorized into

$$\begin{aligned}
&\langle E^\dagger(\bar{t}_s)E(\bar{t}_s)\rangle\langle E^\dagger(\bar{t}_i)E(\bar{t}_i)\rangle\\
&= \left(\sum_k \sinh^2(r_k)\left(u_k(\bar{t}_s)u_k^*(\bar{t}_s)+v_k(\bar{t}_s+\delta t)v_k^*(\bar{t}_s+\delta t)\right)\right)
\end{aligned} \tag{22}$$

$$\times\left(\sum_k \sinh^2(r_k)\left(u_k(\bar{t}_i)u_k^*(\bar{t}_i)+v_k(\bar{t}_i+\delta t)v_k^*(\bar{t}_i+\delta t)\right)\right). \tag{23}$$

It is the product of the mean photon number squared, and shows no dependence on the coherence properties of the quantum light.

For any given entangled photon pulse, equation (14) depends on five parameters, and is a 5D signal. Equation (21) still is a 3D signal. A simpler 1D signal is generated by integrating out the two detector times $\bar{t}_i$ and $\bar{t}_s$,

$$R(\delta t) = \int \mathrm{d}\bar{t}_i \int \mathrm{d}\bar{t}_s\, S(\bar{t}_i,\bar{t}_s;\delta t). \tag{24}$$

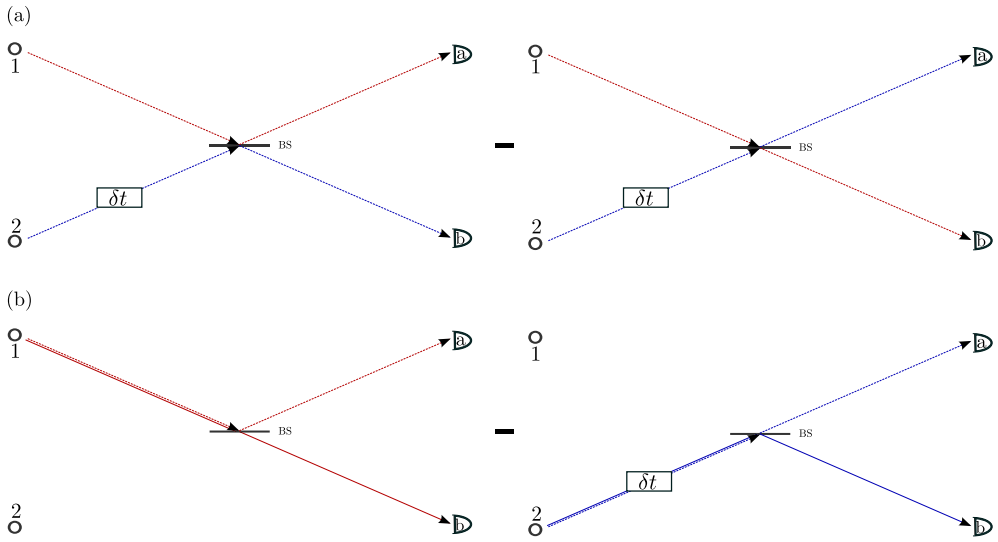

Figure 2. The interfering pathways that create the gated signal (21): (a) pathways responsible for the first term in equation (21). When the twin photons in beams 1 and 2 are indistinguishable, the two diagrams interfere destructively for $\delta t = 0$, creating the HOM-dip in the photon correlation signal. (b) The pathways corresponding to the second term in equation (21). This interference also depends on the indistinguishability of the two beams, but in this case both photons can come from either of the two beams. The third term in equation (21) is not an interference term, and is not depicted.

Substituting equation (21), this yields

$$R(\delta t) = c \int \frac{\mathrm{d}\omega}{2\pi} \int \frac{\mathrm{d}\omega'}{2\pi} \times \{2(|f_{12}(\omega,\omega')|^2 - f_{12}(\omega,\omega') f_{12}^*(\omega',\omega)\, \mathrm{e}^{\mathrm{i}(\omega'-\omega)\delta t}) + |g_1(\omega,\omega')\, \mathrm{e}^{-\mathrm{i}\omega\delta t} - g_2(\omega,\omega')\, \mathrm{e}^{-\mathrm{i}\omega'\delta t}|^2 + [g_1(\omega,\omega) + g_2(\omega,\omega)] \times [g_1(\omega',\omega') + g_2(\omega',\omega')]\}, \quad (25)$$

where

$$f_{12}(\omega,\omega') = \sum_k \psi_k(\omega) \sinh(r_k) \cosh(r_k) \phi_k(\omega'), \quad (26)$$

$$g_1(\omega,\omega') = \sum_k \psi_k(\omega) \sinh^2(r_k) \psi_k^*(\omega'), \quad (27)$$

$$g_2(\omega,\omega') = \sum_k \phi_k(\omega) \sinh^2(r_k) \phi_k^*(\omega'). \quad (28)$$

To study the variation of the photon counting signals with the pump intensity, we choose the normalization factor c in equation (25) such that (25) approaches unity for $\delta t \to \infty$. This signal is depicted in figure 3. We first discuss the contribution of the two-photon state. For pump pulses with very narrow pump bandwidth (i.e. strong entanglement) as depicted in figures 3(a) and (b), one can obtain an almost perfect HOM-dip at zero time delay, provided the two beams are indistinguishable (i.e. $\omega_1 = \omega_2$). For a pump bandwidth of 10 cm^{-1}, the two plots for entanglement times 10 fs (figure 3(a)) and 100 fs (figure 3(b)) look identical, which can be explained by the strong frequency anti-correlations induced by the entanglement. As shown in [34], a larger pump bandwidth leads to an asymmetry between the spectral distribution of the two beams, which renders them distinguishable. This is why for $\sigma_p = 50$ cm^{-1} the entanglement time has a strong influence on the HOM-dip. For $T = 10$ fs, the dip is very narrow, and shows fast oscillations (note the different time axis compared to figures 3(a) and (b)). This is due to the large bandwidth of the two beams, which allows for greater differences in the two beam bandwidths. Consequently, for $T = 100$ fs shown in figure 3(d) the dip is far broader, and no longer shows these fast oscillations. As we increase the pump intensity α, the dip is diminished. This stems from the incoherent autocorrelation contribution in the second line of equation (A.11), where the two detection events originate from two uncorrelated photons. In this case, the broad bandwidth of the individual beams renders it very unlikely to obtain indistinguishable photons.

To further clarify these findings, we depict in figure 4(a) the minimum of the HOM-dip versus the pump intensity represented by $|\alpha|^2$ for entanglement times of 10 and 100 fs. Clearly, in the former case the HOM-dip decreases much faster with an increasing pump intensity. Again, this can be explained by the large bandwidth of the individual beams: the HOM-dip depends on the symmetry between the two detected photon wavepackets, and the broader the bandwidth of the two, the harder it is to achieve perfect overlap of both wavefunctions. Figure 4(b) shows the same quantity for two broadband beams with different pump bandwidths. For larger pump bandwidth, i.e. weaker frequency entanglement, the dip decreases faster. This can be again attributed to the indistinguishability of photons. The sum of the two photon frequencies is distributed over the pump bandwidth. Thus, if one photon is detected at $\omega_p/2+\Omega$ for small pump bandwidths, the other photon will be narrowly distributed around $\omega_p/2-\Omega$. The two photons only interfere for small Ω, so the smaller

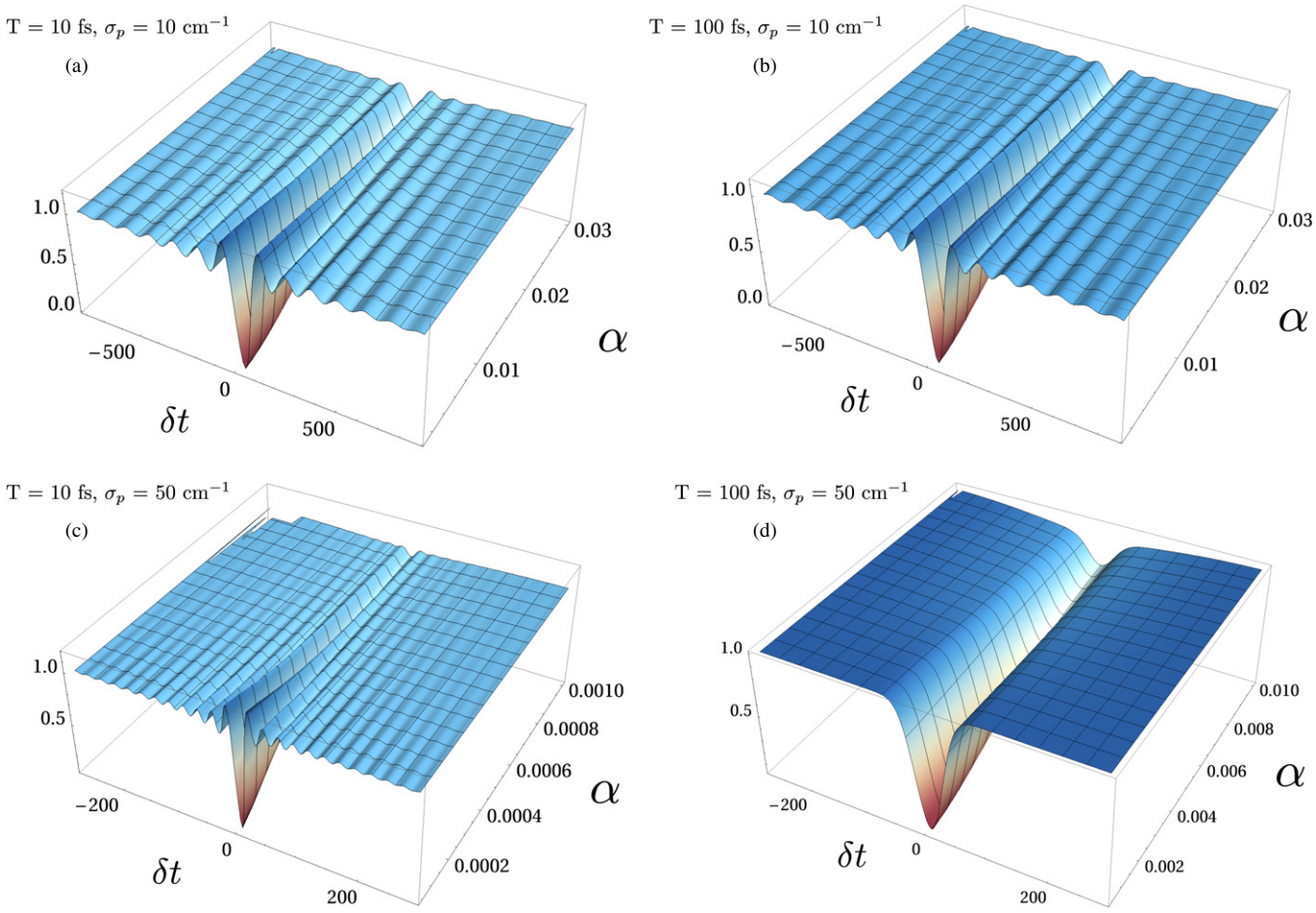

Figure 3. (a) and (b) The photon coincidence signal equation (25) for $\omega_1 = \omega_2 = 11\,000$ cm^{-1} and $\sigma_p = 10$ cm^{-1} plotted versus the pump field intensity parameter α and the delay δt. (c) and (d) The same signal for a broader pump bandwidth $\sigma_p = 50$ cm^{-1}.

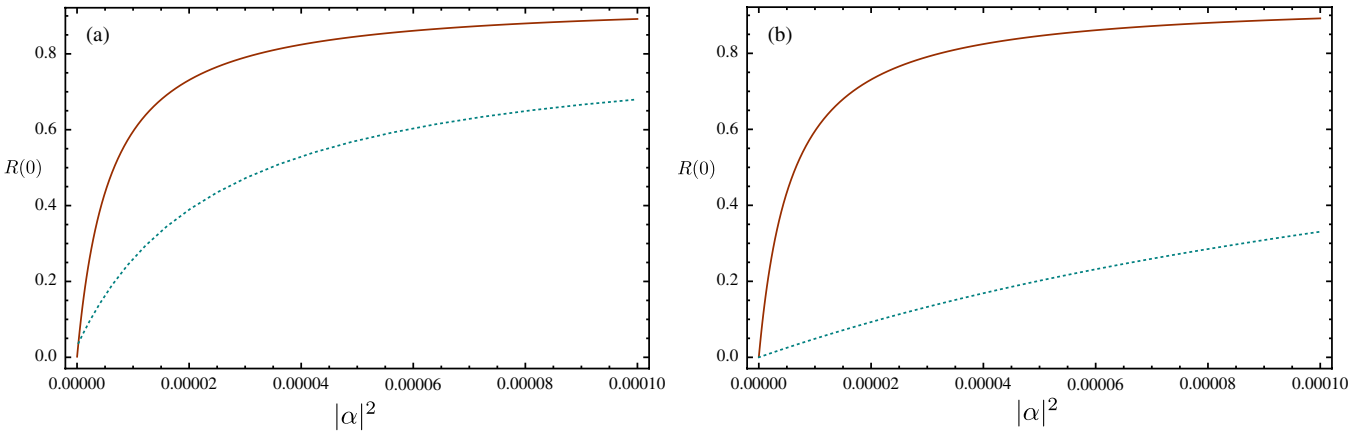

Figure 4. (a) The minimum of the HOM-dip (i.e. $R(\delta t = 0)$) for ideal time gating, equation (25), plotted versus the pump intensity for two beams with pump bandwidth $\sigma_p = 50$ cm^{-1}, and entanglement times $T = 10$ fs (red) and 100 fs (blue, dashed). (b) Same as (a), but for entanglement time $T = 10$ fs and pump bandwidths $\sigma_p = 50$ cm^{-1} (red) and 10 cm^{-1} (blue, dashed).

the bandwidth of the individual beams and the smaller the pump bandwidth the more robust the HOM-dip appears. Thus, strong time–frequency entanglement (i.e. short entanglement time and narrow pump bandwidth) is not always beneficial for sustaining the interference.

4. Ideal frequency gating

Ideal frequency gating is obtained by taking the infinity in the detector spectrogram, and thus

$$e^{-\frac{(t-\bar{t})^2}{\bar{T}^2}} \longrightarrow 1, \tag{29}$$

and

$$\mathrm{e}^{-\frac{(\omega-\bar{\omega})^2}{\sigma_D^2}} \longrightarrow \delta(\omega-\bar{\omega}). \tag{30}$$

Carrying out the integrations of equation (14), we obtain the frequency-gated signal

$$\begin{aligned} S_{\mathrm{FG}}(\bar{\omega}_i,\bar{\omega}_s;\delta t) = &\Bigg|\sum_k \sinh(r_k)\cosh(r_k)(\psi_k(\bar{\omega}_i)\phi_k(\bar{\omega}_s) \\ &- \psi_k(\bar{\omega}_s)\phi_k(\bar{\omega}_i)\,\mathrm{e}^{\mathrm{i}(\bar{\omega}_i-\bar{\omega}_s)\delta t})\Bigg|^2 \\ &+\Bigg|\sum_k \sinh^2(r_k)(\psi_k(\bar{\omega}_s)\psi_k^*(\bar{\omega}_i) \\ &- \phi_k(\bar{\omega}_s)\phi_k^*(\bar{\omega}_i)\,\mathrm{e}^{\mathrm{i}(\bar{\omega}_i-\bar{\omega}_s)\delta t})\Bigg|^2 \\ &+\sum_k \sinh^2(r_k)(|\psi_k(\bar{\omega}_i)|^2+|\psi_k(\bar{\omega}_s)|^2) \\ &\times\sum_{k'} \sinh^2(r_{k'})(|\phi_{k'}(\bar{\omega}_i)|^2+|\phi_{k'}(\bar{\omega}_s)|^2). \end{aligned} \tag{31}$$

By integrating out the two detector frequencies $\bar{\omega}_s$ and $\bar{\omega}_i$, we recover equation (25), illustrating that the ideal time-gated and the ideal frequency-gated signals contain the same amount of information. The time- *and* frequency-gated signals discussed next can reveal further information.

4.1. General time- and frequency-gates

Simultaneous time and frequency gating is used in well-established measurement techniques such as FROG or SPIDER [39, 40] in ultrafast spectroscopy. To our knowledge, so far it has not been applied to two-photon counting. Using equation (17) for finite gating parameters T and Ω (and assuming two identical gates), we obtain

$$\begin{aligned} S(t_i,\bar{\omega}_i;t_s,\bar{\omega}_s;\bar{T},\Omega) = &\,2\pi\bar{T}^2\left(\frac{W}{\sigma_D}\right)^2\int\frac{\mathrm{d}\omega_s}{2\pi}\int\frac{\mathrm{d}\omega_i}{2\pi}\int\frac{\mathrm{d}\omega}{2\pi} \\ &\times\int\frac{\mathrm{d}\omega'}{2\pi}\mathrm{e}^{-(\omega_s-\bar{\omega}_s)^2/\sigma_D^2}\,\mathrm{e}^{-(\omega_i-\bar{\omega}_i)^2/\sigma_D^2}\,\mathrm{e}^{-(\omega-\omega_i)^2\bar{T}^2/2-\mathrm{i}(\omega-\omega_i)\bar{t}_i} \\ &\times\mathrm{e}^{-(\omega'-\omega_s)^2\bar{T}^2/2-\mathrm{i}(\omega'-\omega_s)\bar{t}_s} \\ &\times\Bigg[\sum_k \sinh(r_k)\cosh(r_k)(\psi_k(\omega_i)\phi_k(\omega_s)\,\mathrm{e}^{\mathrm{i}\omega_s\delta t} \\ &-\phi_k(\omega_i)\psi_k(\omega_s)\,\mathrm{e}^{\mathrm{i}\omega_i\delta t}) \\ &\times\sum_{k'} \sinh(r_{k'})\cosh(r_{k'})(\psi_{k'}^*(\omega)\phi_{k'}^*(\omega')\,\mathrm{e}^{-\mathrm{i}\omega'\delta t} \\ &-\phi_{k'}^*(\omega)\psi_{k'}^*(\omega')\,\mathrm{e}^{-\mathrm{i}\omega\delta t}) \\ &+\sum_k \sinh^2(r_k)(\psi_k(\omega_i)\psi_k^*(\omega')-\phi_k(\omega_i)\phi_k^*(\omega')\,\mathrm{e}^{-\mathrm{i}(\omega'-\omega_i)\delta t}) \\ &\times\sum_{k'} \sinh^2(r_{k'})(\psi_{k'}(\omega_s)\psi_{k'}^*(\omega)-\phi_{k'}(\omega_s)\phi_{k'}^*(\omega)\,\mathrm{e}^{-\mathrm{i}(\omega-\omega_s)\delta t}) \\ &+\sum_k \sinh^2(r_k)(\psi_k(\omega_i)\psi_k^*(\omega)+\phi_k(\omega_i)\phi_k^*(\omega)\,\mathrm{e}^{-\mathrm{i}(\omega-\omega_i)\delta t}) \\ &\times\sum_{k'} \sinh^2(r_{k'})(\psi_{k'}(\omega_s)\psi_{k'}^*(\omega')+\phi_{k'}(\omega_s)\phi_{k'}^*(\omega')\,\mathrm{e}^{-\mathrm{i}(\omega'-\omega_s)\delta t})\Bigg]. \end{aligned} \tag{32}$$

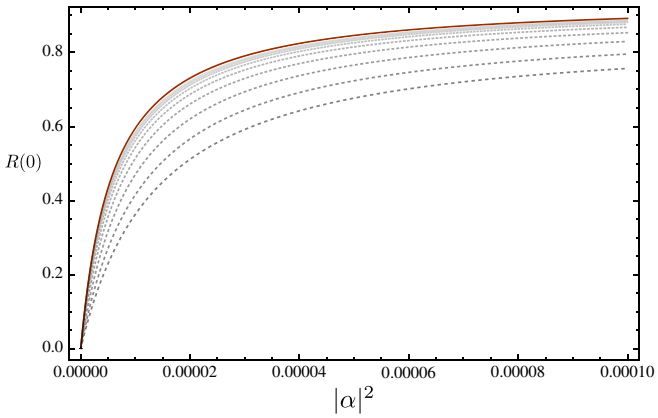

Figure 5. The minimum of the HOM-dip (i.e. $R(\delta t=0)$) for ideal time gating, equation (25), is plotted versus the pump intensity for beams with pump bandwidth $\sigma_p = 50\ \mathrm{cm}^{-1}$, and entanglement time $T = 10$ fs (red). The grey plots show gated signals (equation (33)) with (from bottom to top) $\Omega = 100, \ldots, 800\ \mathrm{cm}^{-1}$ and $\bar{T} = 0.005$ cm.

This has the same three-term structure as the ideal time gating, equation (21), and the corresponding individual contributions can be similarly identified. The detected frequencies are now distributed around $\bar{\omega}_s$ and $\bar{\omega}_i$ with a width σ_D. Consequently, the detection times are not defined precisely, but acquire a $1/\bar{T}$ width.

Using equation (32), the 1D signal (24) becomes

$$\begin{aligned} R(\delta t) = &\int\frac{\mathrm{d}\omega}{2\pi}\int\frac{\mathrm{d}\omega'}{2\pi}\,\mathrm{e}^{-(\omega-\bar{\omega})^2/\sigma_D^2}\,\mathrm{e}^{-(\omega'-\bar{\omega})^2/\sigma_D^2} \\ &\{2(|f(\omega,\omega')|^2 - f(\omega,\omega')f^*(\omega',\omega)\,\mathrm{e}^{\mathrm{i}(\omega'-\omega)\delta t}) \\ &+|g_1(\omega,\omega')\,\mathrm{e}^{-\mathrm{i}\omega\delta t} - g_2(\omega,\omega')\,\mathrm{e}^{-\mathrm{i}\omega'\delta t}|^2 \\ &+[g_1(\omega,\omega)+g_2(\omega,\omega)][g_1(\omega',\omega')+g_2(\omega',\omega')]\}. \end{aligned} \tag{33}$$

Comparison with equation (25) shows that perfect time gating is a reasonable approximation as long as the width of the detector resolution σ_D is much larger than the spectral width of the functions f and g. This does not apply for broadband pulses, when a large number of modes contribute to the signal. As shown in appendix B, these modes k can be described by Hermite functions, and their variance grows with the square root of the index k. This is illustrated in figure 5, where we plot the maximum HOM-dip for a broadband-entangled beam versus the pump intensity for different gates.

In the previous section, we had shown that the broad bandwidth leads to a rapid degradation of the dip, since the two beams become distinguishable. Here, we see that frequency gating can restore the dip to some extent: for a broad gate ($\Omega = 800\ \mathrm{cm}^{-1}$) the plot coincides with the ideal gating case in red. As the frequency gate is narrowed, the dip is degraded more slowly. Thus, by narrow frequency gating, the indistinguishability can be restored to some extent (of course, the total number of coincident counts will be affected by this procedure [34]).

While equation (33) constitutes a generalization of equation (25), it only involves two frequency integrations, and therefore does not carry more information on the four-point correlation function. Instead, we have to go back to equation (32).

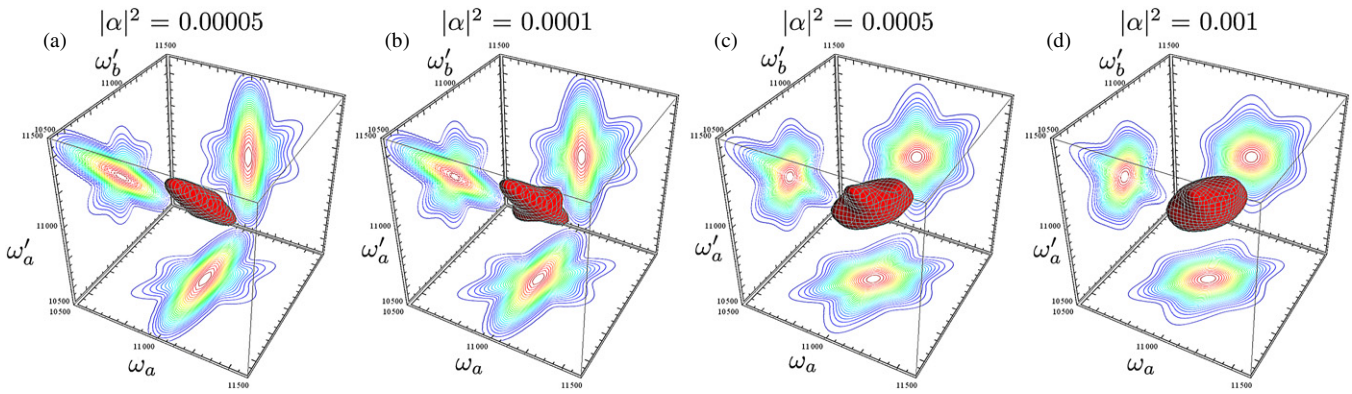

Figure 6. The four-point field correlation function in the frequency domain, $\langle E^\dagger(\omega_a')E^\dagger(\omega_b')E(\omega_b = 11\,000\ \mathrm{cm}^{-1})E(\omega_a)\rangle$, equation (A.13). The pulse parameters are $\omega_1 = \omega_2 = \omega_p/2 = 11\,000\ \mathrm{cm}^{-1}$, $\sigma_p = 50\ \mathrm{cm}^{-1}$ and $T = 100$ fs. The pump intensity is increased from left to right: (a) $|\alpha|^2 = 0.000\,05$, (b) 0.0001, (c) 0.0005 and (d) 0.001.

5. Two-photon absorption

As noted in the introduction, entangled photons hold promise as novel spectroscopic tools. Traditional quantum optics techniques such as the HOM measurement are designed to probe properties of the entangled two-photon wavepackets. Spectroscopic applications, on the other hand, aim at using the nonclassical properties of entangled photons to probe properties of molecular systems. However, in either case the signal depends on the same four-point correlation function of the electric field. In this section, we discuss the influence of the pump intensity on nonlinear spectroscopic signals.

The most common spectroscopic signal, in which this has been investigated, is two-photon-induced fluorescence (TPIF) [7, 8, 29, 41]. In this measurement, a bright state f is excited through the absorption of two photons, where the intermediate state is typically far off-resonant, and the fluorescence from state f is collected. The TPA of entangled photons scales linearly with the pump intensity (rather than quadratically for classical light), and the crossover to the scaling with higher orders shows the break-down of the validity of the two-photon state approximation. Here, we will investigate this crossover and its dependence on the intermediate state.

We calculate the TPA signal with an intermediate state e with variable energy, and a final state f with $21\,000\ \mathrm{cm}^{-1}$. The states are broadened by $\gamma_e = \gamma_f = 200\ \mathrm{cm}^{-1}$. The dipole moments connecting the states were chosen to be $\mu_{ge} = \mu_{ef} = 1$. The signal is proportional to the f-state population after excitation by the entangled beams, which is given by [15]

$$p_f(t;\Gamma) \propto \int^t \mathrm{d}\tau_4 \int^{\tau_4} \mathrm{d}\tau_3 \int^t \mathrm{d}\tau_2 \int^{\tau_2} \mathrm{d}\tau_1 \times \langle V(\tau_3)V(\tau_4)B_f(t)V^\dagger(\tau_2)V^\dagger(\tau_1)\rangle \times \langle E^\dagger(\tau_3)E^\dagger(\tau_4)E(\tau_2)E(\tau_1)\rangle, \tag{34}$$

where

$$B_f(t) = |f(t)\rangle\langle f(t)|, \tag{35}$$

and Γ denotes the set of control parameters such as central frequencies, bandwidths, etc. $V(t)$ denotes the exciton annihilation operator in the interaction picture. Carrying out the time integrations in complete analogy to the previous section, we arrive at

$$p_f(t;\Gamma) \propto \int \frac{\mathrm{d}\omega_a'}{2\pi} \int \frac{\mathrm{d}\omega_b'}{2\pi} \int \frac{\mathrm{d}\omega_a}{2\pi} \int \frac{\mathrm{d}\omega_b}{2\pi}\, \mathrm{e}^{\mathrm{i}(\omega_a'+\omega_b'-\omega_a-\omega_b)t} \times \langle E^\dagger(\omega_a')E^\dagger(\omega_b')E(\omega_b)E(\omega_a)\rangle \times T_{fg}^*(\omega_a',\omega_b')T_{fg}(\omega_a,\omega_b), \tag{36}$$

where we had defined the transition amplitude

$$T_{fg}(\omega_a,\omega_b) = \frac{\mu_{ge}}{\omega_a - \omega_{eg} + \mathrm{i}\gamma_e} \frac{\mu_{ef}}{\omega_a + \omega_b - \omega_{fg} + \mathrm{i}\gamma_f}. \tag{37}$$

In the following, we will study how the four-point correlation function in equation (36) scales with the pump intensity, how its properties change, and how this is reflected in the TPA signal.

5.1. The frequency-domain four-point correlation function

The four-point field correlation function in equation (36) is derived in appendix A. To illustrate the strong frequency correlations present in the entangled twin-photon state, we plot cuts of the four-point correlation function $\langle E^\dagger(\omega_a')E^\dagger(\omega_b')E(\omega_b)E(\omega_a)\rangle$. It is given by equation (A.13), which is symmetric with respect to ω_a and ω_b. We therefore fix ω_b on resonance with the central frequency of the degenerate beams $\omega_p/2$, and plot the absolute value of (A.13) versus the remaining three variables in figure 6. The red three-dimensional contour depicts the equipotential surface at half the maximum value, and the contour plots on the sides depict projections on the corresponding plane spanned by the two variables. These two-dimensional plots are scaled nonlinearly (the colour scale grows as sinh) to better highlight small features. At low intensities in figure 6(a), we can see that ω_a' and ω_b' are strongly anti-correlated. This yields a broad resonance along each of the two frequencies on the planes spanned with ω_a, where we do not see any correlation between the frequencies. This indicates that at this intensity the entangled twin-photon state describes the state of the light very well. It is signified by strong anti-correlations between ω_a' and ω_b', as well as between ω_a and ω_b (which cannot be seen in figure 6). As the pump intensity is increased in figures 6(b)–(d), we observe that the equipotential surface, which looks cigar-shaped for

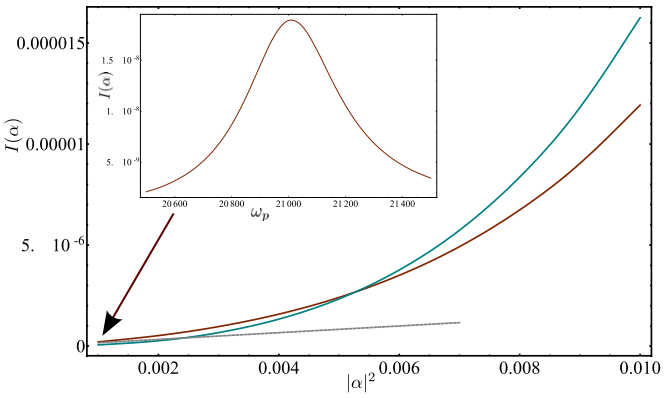

Figure 7. Equation (36) on resonance is plotted versus the pump intensity $|\alpha|^2$ with an off-resonant intermediate state at $e = 12\,500\ \mathrm{cm}^{-1}$. The coherent (red) and the incoherent (blue) contributions are plotted separately. The dashed, grey line is the linear approximation of the coherent term. Inset: equation (36) versus the pump frequency ω_p for $T = 100$ fs, $\sigma_p = 10\ \mathrm{cm}^{-1}$ and $|\alpha|^2 = 0.001$.

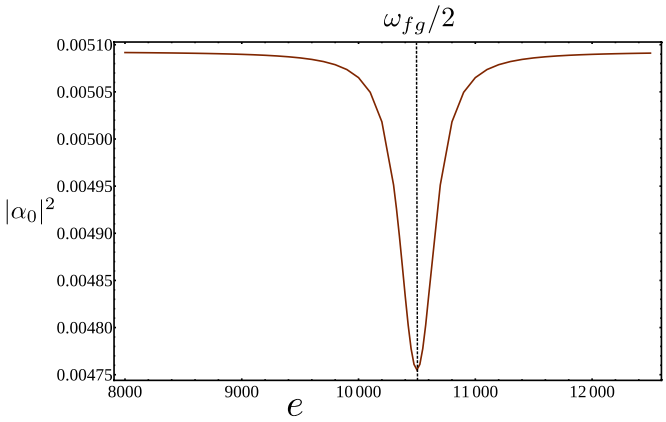

Figure 8. Variation of the intensity $|\alpha_0|^2$, where the coherent and the incoherent contributions cross (see figure 7) with the energy of the intermediate state e.

the two-photon state, develops a broad spherical resonance around the central frequency of the beams. This new feature stems from pairs of uncorrelated photons, and it is responsible for the crossover in the intensity dependence. Note that the crossover in the four-point correlation function happens at a lower intensity than the crossover in the next subsection. This is because we use a pump bandwidth of 50 cm^{-1} (i.e. weaker entanglement) to make the plots look nicer.

5.2. The intensity crossover

The crossover between the linear and nonlinear regimes shows up in the dependence of the TPIF signal on the pump intensity. Equation (A.13) shows that the four-point correlation function contains two contributions: one that stems from the coherent interaction of pairs of entangled photons, and that scales linearly in the pump intensity for low conversion efficiency α. The other 'incoherent' contribution arises from the interaction with one of the two beams and scales quadratically in the pump intensity. Figure 7 depicts equation (36), where ω_p is set on resonance with state f, versus the pump intensity $|\alpha|^2$. The two contributions are plotted separately, and the two-photon state approximation is shown as a dashed line. For low intensities, the coherent contribution dominates the signal, and is well-approximated by the linear approximation. At $|\alpha|^2 \sim 0.003$, the incoherent term becomes stronger than the linear one, and the total signal depends quadratically on the pump intensity. However, even though the signal may no longer be described by the two-photon state, the coherent contribution still dominates, until at $|\alpha_0|^2 \sim 0.0051$, the incoherent term crosses the coherent term, and starts to dominate the signal. Hence, even though the linear scaling breaks down at $|\alpha|^2 = 0.003$, the nonclassical time-bandwidth properties of entangled photon pairs still dominate the signal until the intensity is almost twice as high.

We further investigate how this crossover depends on the intermediate state e [42]. To do this, we plot the crossover intensity $|\alpha_0|^2$ versus the energy of the intermediate state e in figure 8. Clearly, there is a pronounced dip in the crossover intensity, when the state is on resonance with the central frequency of the two beams. This can be rationalized by the strong time correlation between entangled photons. If one of the photons is absorbed, the other one has to arrive within the entanglement time, and thereby foster off-resonant transitions. The incoherent contribution shows no such correlations, and consequently its contribution is enhanced, when the intermediate state is on resonance and the arrival time of the second photon is less important for the signal. The crossover then occurs at lower pump intensities.

6. Conclusions

We have investigated the dependence of the time- and frequency-gated HOM-dip and the TPA signal on the intensity of a pump pulse generating entangled photon pairs. The crossover from the linear intensity scaling of the four-point correlation function signifying an entangled two-photon state to higher powers degrades the HOM-dip, but strongly depending on the beam bandwidths. We further discussed the TPA signal. We find that the crossover of the intensity scaling does not coincide with the crossover in the properties of the beams. Only for an intensity almost twice as high as the intensity crossover, the autocorrelation contribution of each beam becomes more dominant than the coherent interaction of entangled photon pairs. Furthermore, the crossover depends on whether or not the intermediate state is on resonance with the single-photon transitions.

Acknowledgments

We would like to thank J Biggs for helpful discussions. We gratefully acknowledge the support of the National Science Foundation through grant no. CHE-1058791, and the Chemical Sciences, Geosciences and Biosciences Division, Office of Basic Energy Sciences, Office of Science, US Department of Energy.

Appendix A. The four-point field correlation function

We shall calculate the four-point correlation function in the frequency domain

$$\left\langle E^{\dagger}(\omega_a')E^{\dagger}(\omega_b')E(\omega_b)E(\omega_a)\right\rangle, \tag{A.1}$$

where $E(\omega) = E_1(\omega) + E_2(\omega)$. We propagate the field operators in the Heisenberg picture,

$$E_{\mathrm{H}} = U_{\mathrm{PDC}}^{\dagger} E_{\mathrm{S}} U_{\mathrm{PDC}}, \tag{A.2}$$

where in this appendix the subscripts H ans S denote the Heisenberg and Schrödinger pictures, respectively. The functions $\{\psi_k\}$ and $\{\phi_k\}$ in equation (9) form orthonormal bases, known as Schmidt modes, and their mode operators are given by

$$A_k = \int \mathrm{d}\omega_a \psi_k(\omega_a) a(\omega_a) \quad \text{and} \quad B_k = \int \mathrm{d}\omega_b \phi_k(\omega_b) b(\omega_b). \tag{A.3}$$

In this basis, the unitary evolution operator (2) reads

$$\begin{aligned} U_{\mathrm{PDC}} &= \exp\left[\sum_k r_k A_k^{\dagger} B_k^{\dagger} - \mathrm{h.c.}\right] \\ &= \bigotimes\nolimits_k \exp\left[r_k A_k^{\dagger} B_k^{\dagger} - \mathrm{h.c.}\right]. \end{aligned} \tag{A.4}$$

This means that 'the down-conversion generates a tensor product of distinct broadband twin beam squeezers' [19]. For weak down-conversion, i.e. $r_k \ll 1$, the exponential in (A.4) can be expanded, and we recover the entangled two-photon state.

For an arbitrary conversion strength, the action of the transformation (A.4) on the photon annihilation operators is described by input–output relations,

$$A_{k,\mathrm{out}} = U_{\mathrm{PDC}}^{\dagger} A_{k,\mathrm{in}} U_{\mathrm{PDC}} = \cosh(r_k) A_{k,\mathrm{in}} + \sinh(r_k) B_{k,\mathrm{in}}^{\dagger}, \tag{A.5}$$

$$B_{k,\mathrm{out}} = U_{\mathrm{PDC}}^{\dagger} B_{k,\mathrm{in}} U_{\mathrm{PDC}} = \cosh(r_k) B_{k,\mathrm{in}} + \sinh(r_k) A_{k,\mathrm{in}}^{\dagger}. \tag{A.6}$$

In the Schrödinger picture, the electric field is given by

$$E_1(t) = \sum_k A_{k,\mathrm{out}}\, u_k(t), \tag{A.7}$$

and similarly for $E_2(t) = \sum_k B_{k,\mathrm{out}}\, v_k(t)$, where the functions u_k and v_k are given by equations (10) and (11).

We assume that fields 1 and 2 are initially in the vacuum state. Only six terms then survive in the field correlation function of equation (36):

$$\begin{aligned} &\langle E^{\dagger}(\omega_a')E^{\dagger}(\omega_b')E(\omega_b)E(\omega_a)\rangle \\ &\quad = \langle E_1^{\dagger}(\omega_a')E_1^{\dagger}(\omega_b')E_1(\omega_b)E_1(\omega_a)\rangle \\ &\qquad + \langle E_2^{\dagger}(\omega_a')E_2^{\dagger}(\omega_b')E_2(\omega_b)E_2(\omega_a)\rangle \\ &\qquad + \langle E_1^{\dagger}(\omega_a')E_2^{\dagger}(\omega_b')E_2(\omega_b)E_1(\omega_a)\rangle \\ &\qquad + \langle E_1^{\dagger}(\omega_a')E_2^{\dagger}(\omega_b')E_1(\omega_b)E_2(\omega_a)\rangle \\ &\qquad + \langle E_2^{\dagger}(\omega_a')E_1^{\dagger}(\omega_b')E_2(\omega_b)E_1(\omega_a)\rangle \\ &\qquad + \langle E_2^{\dagger}(\omega_a')E_1^{\dagger}(\omega_b')E_1(\omega_b)E_2(\omega_a)\rangle. \end{aligned} \tag{A.8}$$

We next evaluate the third term in equation (A.8). The other terms can be calculated similarly. Using equations (A.5) and (A.6), we obtain in the Heisenberg picture

$$\begin{aligned} &\langle\psi_i|E_{1,H}^{\dagger}(\omega_a')E_{2,H}^{\dagger}(\omega_b')E_{2,H}(\omega_b)E_{1,H}(\omega_a)|\psi_i\rangle \\ &\quad = \sum_{k,k',k'',k'''} \psi_k(\omega_a')\phi_{k'}(\omega_b')\phi_{k''}^{*}(\omega_b)\psi_{k'''}^{*}(\omega_a) \\ &\quad \langle 0|(\cosh(r_k)A_k^{\dagger} + \sinh(r_k)B_k)(\cosh(r_{k'})B_{k'}^{\dagger} + \sinh(r_{k'})A_{k'}) \\ &\quad \times (\cosh(r_{k''})B_{k''} + \sinh(r_{k''})A_{k''}^{\dagger}) \\ &\quad \times (\cosh(r_{k'''})A_{k'''} + \sinh(r_{k'''})B_{k'''}^{\dagger})|0\rangle. \end{aligned} \tag{A.9}$$

This correlation function does not vanish, since in (A.5) and (A.6) photon creation and annihilation operators are mixed. Only 2 of the 16 terms above are finite, $\propto \langle B_k B_{k'}^{\dagger} B_{k'} B_{k'''}^{\dagger}\rangle = \delta_{k,k'}\delta_{k'',k'''}$ and $\propto \langle B_k A_{k'} A_{k''}^{\dagger} B_{k'''}^{\dagger}\rangle = \delta_{k,k'''}\delta_{k',k''}$, which immediately yields the final result,

$$\begin{aligned} &\langle E_1^{\dagger}(\omega_a')E_2^{\dagger}(\omega_b')E_2(\omega_b)E_1(\omega_a)\rangle \\ &\quad = \sum_k \sinh(r_k)\cosh(r_k)\psi_k(\omega_a')\phi_k(\omega_b') \\ &\quad \times \sum_{k'} \sinh(r_{k'})\cosh(r_{k'})\phi_{k'}^{*}(\omega_b)\psi_{k'}^{*}(\omega_a) \end{aligned} \tag{A.10}$$

$$+ \sum_{k,k'} \sinh^2(r_k)\psi_k(\omega_a')\psi_k^{*}(\omega_a)\sinh^2(r_{k'})\phi_{k'}(\omega_b')\phi_{k'}^{*}(\omega_b). \tag{A.11}$$

The pump intensity is given by $I = |A_0|^2$. The singular values r_k in equation (9) are proportional to the conversion efficiency α, and therefore $r_k \propto \sqrt{I}$. For low conversion efficiency, $r_k \ll 1$, we can approximate $\sinh(r_k) \simeq r_k$ and $\cosh(r_k) \simeq 1$. This allows us to write

$$\begin{aligned} &\sum_{k,k'} \sinh(r_k)\cosh(r_k)\sinh(r_{k'}) \\ &\quad \times \cosh(r_{k'})\psi_k(\omega_a')\phi_k(\omega_b')\phi_{k'}^{*}(\omega_b)\psi_{k'}^{*}(\omega_a) \\ &\quad \approx \sum_k \psi_k(\omega_a')r_k\phi_k(\omega_b')\phi_{k'}^{*}(\omega_b)r_{k'}\psi_{k'}^{*}(\omega_a) \\ &\quad = \left(-\frac{\mathrm{i}}{\hbar}\right)^2 \Phi^{*}(\omega_a', \omega_b')\Phi(\omega_a, \omega_b), \end{aligned} \tag{A.12}$$

which coincides with the result we obtain for the twin-photon state [15]. The second term in equation (A.11) has the leading order contribution $\propto r_k^2$, and can therefore be neglected for low conversion efficiency α. The first term in equation (A.11) is to leading order linear in the pump intensity, it corresponds to the coherent interaction of entangled photon pairs and we will refer to it as the 'coherent' term. The second term in equation (A.11) depends quadratically on I. Therefore, it stems from the incoherent contributions from either of the two beams, and will be denoted the 'incoherent term'.

Repeating the same steps for correlation functions in equation (A.8), we can combine the six terms in equation (A.8), and write

$$\begin{aligned} &\langle E^{\dagger}(\omega_a')E^{\dagger}(\omega_b')E(\omega_b)E(\omega_a)\rangle = f^{*}(\omega_a', \omega_b')f(\omega_a, \omega_b) \\ &\qquad + g(\omega_a, \omega_a')g(\omega_b, \omega_b') + g(\omega_a, \omega_b')g(\omega_b, \omega_a'), \end{aligned} \tag{A.13}$$

where

$$\begin{aligned} f^{*}(\omega, \omega') &= \sum_k \sinh(r_k)\cosh(r_k) \\ &\quad \times (\psi_k(\omega)\phi_k(\omega') + \phi_k(\omega)\psi_k(\omega')), \end{aligned} \tag{A.14}$$

$$g(\omega,\omega') = \sum_k \sinh^2(r_k)(\psi_k(\omega)\psi_k^*(\omega') + \phi_k(\omega)\phi_k^*(\omega')). \tag{A.15}$$

Note that the coherent term $f(\omega,\omega')$ correlates two absorption or emission events, and always involves an interaction with a photon from both beams. $g(\omega,\omega')$ correlates absorption with emission, and both interactions stem from either of the two beams.

Appendix B. Analytic SVD

When we neglect the minor maxima of the sinc-function in equation (6), we can approximate it by a Gaussian function,

$$\operatorname{sinc}\left(\frac{\Delta k(\omega_a,\omega_b)L}{2}\right) \simeq \exp\left(-\gamma(\Delta k(\omega_a,\omega_b)L)^2\right), \tag{B.1}$$

with the constant $\gamma = 0.048\,22$. If we further use a Gaussian envelope for the pump pulse,

$$A_p(\omega_a+\omega_b) = \frac{1}{\sqrt{2\pi\sigma_p^2}}\exp\left(-\frac{(\omega_a+\omega_b-\omega_p)^2}{2\sigma_p^2}\right), \tag{B.2}$$

where ω_p is the central pump frequency, the entire two-photon amplitude equation (6) is given by two Gaussian functions. Now we can employ the following identity to carry out the SVD (equation (9)) analytically [43–45]:

$$-\frac{\mathrm{i}\alpha}{\hbar\sqrt{2\pi\sigma_p^2}}\exp[-ax^2-2bxy-cy^2] = \sum_{n=0}^{\infty} r_n H_n(k_1x)H_n^*(k_2y), \tag{B.3}$$

with

$$r_n = \frac{\alpha}{\hbar}\sqrt{\frac{1+\mu^2}{4ac\sigma_p^2}}\mu^n, \tag{B.4}$$

and

$$H_n(kx) = \sqrt{\frac{k}{2^n(n!)\sqrt{\pi}}}\,\mathrm{e}^{\mathrm{i}\frac{3\pi}{8}-(kx)^2}h_n(kx), \tag{B.5}$$

where h_n denotes the nth Hermite polynomial, $\mu = (-\sqrt{ac}+\sqrt{ac-b^2})/b$, $k_1 = \sqrt{2a(1-\mu^2)/(1+\mu^2)}$ and $k_2 = \sqrt{2c(1-\mu^2)/(1+\mu^2)}$. The Hermite functions are normalized, such that

$$\int \mathrm{d}x|H_n(kx)|^2 = 1. \tag{B.6}$$

With the two exponentials (B.1) and (B.2), we have $a = 1/(2\sigma_p^2)+\gamma T_1^2$, $b = 1/(2\sigma_p^2)+\gamma T_1T_2$ and $c = 1/(2\sigma_p^2)+\gamma T_2^2$.

This decomposition was used to evaluate the field correlation functions throughout this paper.

References

[1] Gisin N, Ribordy G, Tittel W and Zbinden H 2002 Quantum cryptography *Rev. Mod. Phys.* **74** 145–95

[2] Boyd R W and Bentley S J 2006 Recent progress in quantum and nonlinear optical lithography *J. Mod. Opt.* **53** 713–8

[3] Giovannetti V, Lloyd S and Maccone L 2011 Advances in quantum metrology *Nature Photon.* **5** 222–9

[4] Horodecki R, Horodecki P, Horodecki M and Horodecki K 2009 Quantum entanglement *Rev. Mod. Phys.* **81** 865–942

[5] Lvovsky A I and Raymer M G 2009 Continuous-variable optical quantum-state tomography *Rev. Mod. Phys.* **81** 299–332

[6] Polzik E S, Carri J and Kimble H J 1992 Spectroscopy with squeezed light *Phys. Rev. Lett.* **68** 3020–3

[7] Lee D-I and Goodson T 2006 Entangled photon absorption in an organic porphyrin dendrimer *J. Phys. Chem.* B **110** 25582–5

[8] Guzman A R, Harpham M R, Suzer O, Haley M M and Goodson T G 2010 Spatial control of entangled two-photon absorption with organic chromophores *J. Am. Chem. Soc.* **132** 7840–1

[9] Kira M, Koch S W, Smith R P, Hunter A E and Cundiff S T 2011 Quantum spectroscopy with Schrödinger-cat states *Nature Phys.* **7** 799–804

[10] Fei H-B, Jost B M, Popescu S, Saleh B E A and Teich M C 1997 Entanglement-induced two-photon transparency *Phys. Rev. Lett.* **78** 1679–82

[11] Saleh B E A, Jost B M, Fei H-B and Teich M C 1998 Entangled-photon virtual-state spectroscopy *Phys. Rev. Lett.* **80** 3483–6

[12] Roslyak O, Marx C A and Mukamel S 2009 Nonlinear spectroscopy with entangled photons: manipulating quantum pathways of matter *Phys. Rev.* A **79** 033832

[13] Roslyak O and Mukamel S 2009 Multidimensional pump-probe spectroscopy with entangled twin-photon states *Phys. Rev.* A **79** 063409

[14] Richter M and Mukamel S 2010 Ultrafast double-quantum-coherence spectroscopy of excitons with entangled photons *Phys. Rev.* A **82** 013820

[15] Schlawin F, Dorfman K E, Fingerhut B P and Mukamel S 2012 Manipulation of two-photon-induced fluorescence spectra of chromophore aggregates with entangled photons: a simulation study *Phys. Rev.* A **86** 023851

[16] de J Len-Montiel R, Svozilk J, Salazar-Serrano L J and Torres J P 2013 Role of the spectral shape of quantum correlations in two-photon virtual-state spectroscopydel *New J. Phys.* **15** 053023

[17] Glauber R J 2007 *Quantum Theory of Optical Coherence* (Berlin: Wiley-VCH)

[18] Cohen-Tannoudji C and Guéry-Odelin D 2011 *Advances In Atomic Physics: An Overview* (Singapore: World Scientific)

[19] Christ A, Laiho K, Eckstein A, Cassemiro K N and Silberhorn C 2011 Probing multimode squeezing with correlation functions *New J. Phys.* **13** 033027

[20] Christ A, Brecht B, Mauerer W and Silberhorn C 2012 Theory of quantum frequency conversion and parametric down-conversion in the high gain regime *New J. Phys.* **15** 053038

[21] Hong C K and Mandel L 1985 Theory of parametric frequency down conversion of light *Phys. Rev.* A **31** 2409–18

[22] Ghosh R, Hong C K, Ou Z Y and Mandel L 1986 Interference of two photons in parametric down conversion *Phys. Rev.* A **34** 3962–68

[23] Olsen M K, Horowicz R J, Plimak L I, Treps N and Fabre C 2000 Quantum-noise-induced macroscopic revivals in second-harmonic generation *Phys. Rev.* A **61** 021803

[24] Olsen M K, Plimak L I and Khoury A Z 2002 Dynamical quantum statistical effects in optical parametric processes *Opt. Commun.* **201** 373–80

[25] Olsen M K, Plimak L I and Khoury A Z 2003 Quantum analysis of the nondegenerate optical parametric amplifier with injected signal *Opt. Commun.* **215** 101–11

[26] Ou Z Y and Mandel L 1988 Violation of Bell's inequality and classical probability in a two-photon correlation experiment *Phys. Rev. Lett.* **61** 50–53
[27] Hong C K, Ou Z Y and Mandel L 1987 Measurement of subpicosecond time intervals between two photons by interference *Phys. Rev. Lett.* **59** 2044–6
[28] Javanainen J and Gould P L 1990 Linear intensity dependence of a two-photon transition rate *Phys. Rev.* A **41** 5088–91
[29] Dayan B, Pe'er A, Friesem A A and Silberberg Y 2005 Nonlinear interactions with an ultrahigh flux of broadband entangled photons *Phys. Rev. Lett.* **94** 043602
[30] Shih Y 2003 Entangled photons *IEEE J. Sel. Top. Quantum Electron.* **9** 1455–67
[31] Pe'er A, Dayan B, Friesem A A and Silberberg Y 2005 Temporal shaping of entangled photons *Phys. Rev. Lett.* **94** 073601
[32] Loudon R 2000 *The Quantum Theory of Light* (Oxford: Oxford University Press)
[33] Roslyak O and Mukamel S 2009 A unified description of sum frequency generation, parametric down conversion and two-photon fluorescence *Mol. Phys.* **107** 265–80
[34] Grice W P and Walmsley I A 1997 Spectral information and distinguishability in type-II down-conversion with a broadband pump *Phys. Rev.* A **56** 1627–34
[35] Law C K, Walmsley I A and Eberly J H 2000 Continuous frequency entanglement: effective finite Hilbert space and entropy control *Phys. Rev. Lett.* **84** 5304–7
[36] Dorfman K E and Mukamel S 2012 *Phys. Rev.* A **86** 013810
[37] Mukamel S, Ciordas-Ciurdariu C and Khidekel V 1996 Wigner spectrograms for femtosecond pulse-shaped heterodyne and autocorrelation measurements *IEEE J. Quantum Electron.* **32** 1278–88
[38] Erdmann R, Branning D, Grice W and Walmsley I A 2000 Restoring dispersion cancellation for entangled photons produced by ultrashort pulses *Phys. Rev.* A **62** 053810
[39] Trebino R 2000 *Frequency-Resolved Optical Gating: The Measurement of Ultrashort Laser Pulses* (Boston, MA: Kluwer–Academic)
[40] Iaconis C and Walmsley I A 1998 Spectral phase interferometry for direct electric-field reconstruction of ultrashort optical pulses *Opt. Lett.* **23** 792–4
[41] Dayan B, Pe'er A, Friesem A A and Silberberg Y 2004 Two photon absorption and coherent control with broadband down-converted light *Phys. Rev. Lett.* **93** 023005
[42] Upton L, Harpham M, Suzer O, Richter M, Mukamel S and Goodson T 2013 Optically excited entangled states in organic molecules illuminate the dark *J. Phys. Chem. Lett.* **4** 2046–52
[43] U'Ren A B, Banaszek K and Walmsley I A 2003 Photon engineering for quantum information processing *Quantum Inform. Comput.* **3** 480–502
[44] Grice W P, U'Ren A B and Walmsley I A 2001 Eliminating frequency and space-time correlations in multiphoton states *Phys. Rev.* A **64** 063815
[45] Maurer W 2009 On colours, keys, and correlations: multimode parametric downconversion in the photon number basis *PhD Thesis* Friedrich-Alexander-Universität Erlangen-Nürnberg